RIVER DISCHARGE AND BATHYMETRY ESTIMATIONS FROM SWOT ALTIMETRY MEASUREMENTS

Kévin Larnier, Jerome Monnier, P.-A. Garambois, J. Verley

RIVER DISCHARGE AND BATHYMETRY ESTIMATIONS FROM SWOT ALTIMETRY MEASUREMENTS

K. LARNIER(1)(2)(3)(4), J. MONNIER(2)(3)*, P.-A. GARAMBOIS(4)(5), J. VERLEY (2)(3)(4)

(1) CS corporation, Business Unit Espace, Toulouse, France.
(2) Institut de Mathématiques de Toulouse (IMT), France.
(3) INSA Toulouse, France.
(4) ICUBE, Strasbourg, France.
(5) INSA Strasbourg, France.
* Corresponding author: jerome.monnier@insa-toulouse.fr

Keywords. Discharge, bathymetry, inference, data assimilation, altimetry, SWOT, ungauged rivers.

Abstract. An inversion algorithm to estimate the discharge of rivers observed by the forthcoming SWOT mission (wide swath altimetry) is elaborated and assessed into details. The algorithm relies on an advanced variational data assimilation formulation applied to the Saint-Venant equations (1D shallow-water) and permanent low Froude flow relations (direct and inverse algebraic models). This hierarchical based modeling approach makes possible to estimate the three key unknowns, that are the time-dependent inflow discharge $Q_{in}(t)$, the space varying bathymetry $b(x)$ and a varying roughness coefficient K, from altimetry measurements only. The flow model is build up from effective cross sections defined from the altimetry measurements. The numerical results are analyzed on three river portions ($\sim$ 100 km long) presenting highly frequent flow variations compared to the observation frequency. Two scenarios of observation are considered: frequent satellite overpasses corresponding to the SWOT Cal-Val orbit ($\sim$1 day period) and SWOT like data corresponding to $\sim$21 days period with 1 to 4 passes at mid-latitudes. The numerical experiments demonstrate that the estimations of the discharge $Q_{in}(t)$ are accurate, the bathymetry profile $b(x)$ too. Various prior configurations of Q and b are considered in view of worldwide applications. Past the learning period (i.e. after the assimilation of a complete measurements set, typically after one year), the low complexity algebraic models provide accurate discharge estimations in real-time from newly acquired measurements.

1. Introduction

While the in-situ observation of the continental water cycle and river flows is declining, a myriad of satellites for earth observations provide more and more accurate measurements. The future Surface Water and Ocean Topography (SWOT) mission (CNES-NASA, planned to be launched in 2021) equipped with a swath mapping radar interferometer will provide river surface mapping at a global scale with an unprecedented spatial and temporal resolution on Water Surface (WS) height, width and slope - decimetric accuracy on WS height averaged over 1 km^2 [57]. SWOT will cover a great majority of the globe with relatively frequent revisits (1 to 4 revisits per 21 days repeat cycle). In complementarity with decades of nadir altimetry on inland waters [12], SWOT should offer the opportunity to increase our knowledge of the spatial and temporal distribution of hydrological fluxes including stream and rivers see e.g.[5, 7]. Thanks to this increased observability of WS worldwide, it will be possible to address a variety of inverse problems in surface hydrology and related fields, see e.g. [51]. Given these WS measurements (elevation, water mask extents), the challenging inverse problems consist to infer the discharge, the unobservable cross sections, but also the friction parametrization and the lateral contributions. The estimation of the discharge is more or less challenging depending on the space-time observations density, the prior information quality and the measurement errors. A relatively recent literature addresses some of these inverse questions including in a pure remote sensing data context, that means sparse in space and time, see e.g. [7] for a review. Few low-complexity methods, based either on steady-state flow models (like the Manning-Strickler's law) or hydraulic geometries (empirical power-laws) have been developed, [8, 22, 25, 67]. In [21], few approaches are compared on 19 rivers with artificially densified daily observables; the results are fluctuating depending on the algorithm tested. No approach turned out to be accurate or robust in all configurations; the benefit of having a correct bathymetry priori estimation is highlighted.

In the river hydraulic community, the most employed data assimilation studies are based on sequential algorithms, the Kalman filter and its variants, see e.g. [59, 56] based on the 1D Saint-Venant model, [49] based on the diffusive wave model, and see e.g. [6, 66, 53, 23] for complete river networks with simplified routing methods. In these studies, the sequential data assimilation algorithms correct the upstream discharge (or potentially a constant roughness coefficient K); none of these study address the challenging inference of the triplet, that is the discharge Q, the bathymetry b and the roughness coefficient K.

The Variational Data Assimilation (VDA) approach, based on the optimal control of the dynamics flow model, see [61, 41, 50, 19] and e.g. [10, 46] for online courses, has demonstrated to be an excellent approach to solve the present inverse problems. The VDA approach consists in minimizing a cost function measuring the discrepancy between the model outputs and the observations; somehow combining in a least square sense the model, the observations and

prior information (potentially available). This approach makes possible to "invert" high-dimensional "control vectors" (the unknown parameters) in highly complex dynamic models. This approach is operational in meteorology and oceanography since the beginning of the century. In river hydraulics, in some circumstances it is possible to infer the key unknown "parameters" of the flow model (inflow discharge $Q_{in}(t)$, bathymetry $b(x)$, roughness K) and/or forcing terms (e.g. lateral fluxes). Among the pioneer VDA studies dedicated to hydraulic models, let us cite [55, 15, 60]; next [4, 34, 14] infered the inflow discharge in 2D shallow water river models. Infering the discharge and the complete set of the hydraulic parameters from WS measurements may be impossible, depending on the flow regime, the adequacy between the observations frequency and the flow dynamics, the prior information. The related equifinality issues are pointed out e.g. in [3]. The inference of the key triplet (inflow discharge, effective bathymetry and friction coefficient) is investigated in [35, 36] but from surface Lagrangian drifting markers providing relatively constraining observations. Based on a real river dataset (Pearl River in China), the upstream, downstream and few lateral fluxes are identified from water levels measured at in-situ gauging stations in [34]; however again the bathymetry and roughness are given. The assimilation of spatially distributed water level observations in a flood plain (a single image acquired by SAR) and a partial in-situ time series (gauging station) are investigated in [39, 37]; see also [48] which presents local sensitivity maps in floodplains making possible to better understand the flow controls and the model, in particular the influence of the bathymetry and local friction coefficient values. In [27, 45] the inference of inflow discharge and lateral fluxes are identified by VDA by superposing a 2D local "zoom model" over the 1D Saint-Venant model; these studies are not conducted in a sparse altimetry measurement context. The altimetry measurements of WS are generally sparse, both in space and time, compared to the flow dynamics. This important feature of the inverse problem is analyzed into details in [11] through the very instructive "identifiability map". The latter is the $(x,t)-$plane representation of all the available information, that are the satellite measurements, the model response in terms of wave propagation and the misfit with the equilibrium state. Concerning the bathymetry inference, it is shown in [28, 25] that given one (1) in-situ measurement of bathymetry, the complete bathymetry profile can be reconstructed, see also [11] with the same VDA approach as the present one. [26, 52, 11] present accurate inferences of $Q(t)$ by a similar VDA process as in the present study but without the present hierarchical modeling approach. However it is important to notice that crucial prior information may be have been implicitly introduced into the direct model; typically in the river case considered in [52] a rating curve $Q(h)$ is imposed at outflow, hence fully controlling the low Froude river flow and imposing the correct prior relation between Q and b; also the important a-priori values of the VDA iterative process are a light Gaussian perturbation only of the "true" values of (K, b). Without a correct prior information on the bathymetry $b(x)$ or the roughness coefficient $K(x)$, the equifinality issue remains, hence not fully solving the inverse problem for ungauged rivers. (Recall that accurate prior information are not available at global scale, see e.g. [2, 17, 1]). However all these relatively recent studies demonstrate the great capabilities of the VDA approach to infer accurately the inflow discharge $Q_{in}(t)$ but do not solve the equifinality issue of the pair $(b(x), K)$ yet.

In view to apply the algorithms to worldwide river portions i.e. in lack of accurate prior information, no prior information can be implicitly introduced into the direct model and enhanced formulations of the inverse model need to be elaborated. If any reliable prior information is available (even a mean value estimation at large scale) then this prior information can be mathematically translated into regularization terms in the VDA formulation, see e.g. [38] for the theory. The present study proposes such improvements in particular by introducing a hierarchical modeling strategy. The approach is based on an advanced VDA process taking into account a-priori scale dependency (covariance operators defined at the adequate hydraulic scale and taking into account the a-priori error amplitudes) applied to the classical 1D Saint-Venant equations (with adequate effective cross-sections) combined with original steady-state low Froude flow systems (direct and inverse low complexity relations). This enriched inverse modeling formulation makes possible to estimate accurately the discharge $Q_{in}(t)$ but also $b(x)$ and $K(h)$ (that is K is regime flow dependent) *without* prior information (since generally not available at global scale yet).

The identified effective cross-sectional shapes are not completely basic since they are super-impositions of the numerous effective trapeziums measured by the satellite instrument. Preliminary analysis based on the identifiability maps introduced in [11] makes possible to adequately define - manually refine the time grid of the identified discharge. The numerical results are presented on three portion rivers, ~ 100 km long. Each case presents a "low identifiability index" (definition in [11]) that is a quite high frequency hydrograph variations compared to the observation frequency; in short a challenging dynamic inverse problem. Two scenarios of observation are considered: 1) a SWOT like Cal-Val orbit with $\sim$1 day period) a SWOT like data with 21 days period (with 1 to 4 passes at mid-latitudes). For each river case and observation scenario, three ancillary data availability configurations are considered; from the most challenging one, ungauged rivers observed by SWOT only, to river portions with reliable in-situ data / database. All the algorithms developed are available in the open-source computational software DassFlow [47].

The outline of the article is as follows. Section 2 presents the dynamic river flow model (Saint-Venant's equations) with the particular cross section shapes, a flow dependent roughness power law $K(h)$, h the water depth (and no prior information in its outflow condition). Section 3 presents the advanced VDA method taking into account prior hydraulic scale and error measurement amplitudes. In Section 4, various low Froude flow relations are re-derived, then providing two original algebraic non-linear systems useful for different purposes. A first use is to estimate quite accurate first values for the iterative VDA process; a second one is to estimate the discharge in real time (once a sufficiently long time series of SWOT observations have been assimilated into the Saint-Venant model, i.e. passed a

"learning period"). The three rivers cases with the few considered scenarios (leading to 16 numerical experiments) are presented in Section 5. The numerical inversions of the triplet $(Q_{in}(t); b(x), K)$ based on long time series (90 to 180 days) of SWOT like measurements are analyzed in Section 6. Section 7 presents real-time estimations of discharge based on the low complexity relations, and passed the "learning period"-calibration process in Section 6. A conclusion is proposed in Section 8.

2. River flow hydrodynamic model

2.1. **1D Saint-Venant equations.** Open channel flows can be accurately described by the 1D Saint-Venant equations in (S, Q) variables, see e.g. [16, 13]. This model is depth-integrated and relies on the long-wave assumption (shallow water). The equations read:

$$\frac{\partial}{\partial t}(\mathbf{U}) + \frac{\partial}{\partial x}(\mathbf{F}) = \mathbf{S_f} \text{ with } \mathbf{U} = \begin{bmatrix} A \\ Q \end{bmatrix}, \mathbf{F} = \begin{bmatrix} Q \\ {}^{Q^2}/_{A} + P \end{bmatrix}, \mathbf{S_f} = \begin{bmatrix} 0 \\ g\int_0^h (h-z)\frac{\partial \tilde{w}}{\partial x}\, dz - gA[\frac{\partial b}{\partial x} + S_f] \end{bmatrix} \tag{2.1}$$

where A is the wetted-cross section $\left[m^2\right]$, Q is the discharge $\left[m^3.s^{-1}\right]$, $P = g\int_0^h (h-z)\tilde{w}dz$ is the pressure term as proposed in [64], $\tilde{w}(z)$ is the WS top width at elevation z $[m]$, g is the gravity magnitude $\left[m.s^{-2}\right]$, Z is the WS elevation $[m]$, $Z = (b + h)$ where b is the lowest bed level $[m]$ and h is the water depth $[m]$. S_f denotes the classical Manning-Strickler law: $S_f = \frac{|Q|Q}{K^2 S^2 R_h^{4/3}}$ with K the Strickler roughness coefficient $\left[m^{1/3}.s^{-1}\right]$, $R_h = {}^{A}/_{P_h}$ the hydraulic radius $[m]$, P_h the wetted perimeter. The discharge Q is related to the average cross sectional velocity u $\left[m.s^{-1}\right]$ such as $Q = uA$. The left-hand side (2.1) is written in its conservative form (hyperbolic operator) while the right-hand side is a "source term". The Strickler roughness coefficient K is defined as a power law in the water depth h:

$$K(h) = \alpha\ h^{\beta} \tag{2.2}$$

where α and β are two constants. This a-priori law makes possible to set the roughness in function of the flow regime; it is richer than a constant uniform value as it is often set in the literature. Also the power-law can be defined by reaches as: $K(r; h) = \alpha_r\ h^{\beta_r}$ with $r$the "reach" number.

Boundary conditions consist to impose the discharge $Q_{in}(t)$ at upstream and the normal depth (estimated from the Manning-Strickler equation) at downstream. The initial condition is set as the steady state backwater curve profile: $Z_0(x) = Z(Q_{in}(t_0))$. This 1D Saint-Venant model is discretized using the classical implicit Preissman scheme, see e.g. [18]. This is implemented into the computational software DassFlow [47].

2.2. **River description from SWOT measurements.** The forthcoming SWOT measurements will provide spatially distributed measurements of river surface elevation Z and width W with temporal revisits [57]. We denote by $(Z_{r,p}, W_{r,p})$ the WS elevation and width for reach r at the satellite overpass p instant. The SWOT WS slope will be calculated at the scale of reaches of several kilometers, [24]). In this study, if required (in the low complexity relations section), the slopes are calculated by finite differences on Z.

We consider R reaches, $r = 1, .., R$, and $(P + 1)$ overpasses, $p = 0, .., P$. The overpasses are ordered by increasing flow height. The case $p = 0$ denotes the lowest water level. The set of SWOT observables on a river domain is the set $(Z_{r,p}, W_{r,p})_{R,P+1}$. The direct model (2.1) is considered with the specific cross sectional geometry indicated in Fig. 2.1. It consists in discrete cross sections formed by asymmetrical trapezium layers $(Z_{r,p}, W_{r,p})$. The center of each flow WS varies; it is denoted by $Y_{r,p}$. In all the sequel we assume that the WS slope $S_{r,p} = -\partial_r Z_{r,p} > 0$.

The cross-sectional areas $A_{r,p}$ are defined as follows: $A_{r,p} = A_{r,0} + \delta A_{r,p} = A_{r,0} + \int_{h_0}^{h_p} W_r(h)dh \ \ \forall r\ \forall p$. The variations $\delta A_{r,p}$ are approximated by the trapeziums $\delta A_{r,p} \approx \sum_{q=1}^{p} \frac{1}{2}(W_r^q + W_r^{q-1})(h_r^q - h_r^{q-1})$. The wetted area $A_{r,0}\, \forall r$ is unobserved.

Moreover we have: $h_{r,p} \approx R_{r,p}^h \approx \frac{A_{r,p}}{W_{r,0}+2h_{r,p}+W_{r,p}}\ \ \forall r$; (this approximation has numerically verified on all text rivers considered in [21]). Since $W >> h$, it follows the effective depth expression: $h_{r,p} = (A_{r,0} + \delta A_{r,p})(W_{r,0} + W_{r,p})^{-1}$. The flows are supposed to be gradually varied that is: $\partial_x W_{r,p}/W_{r,p} \approx 0$.

The unobserved wetted cross section A_0 for a given reach can be represented by a rectangle, a trapezium, a parabola or even a triangle, by setting $A_0 = \alpha_A h_{0,\alpha} W$ with $\alpha_A \in [\frac{1}{2}, 1]$. However it will be shown that the a-priori effective cross-section shape does not influence the low complexity flow relations (see Section 4). Then we define the hydraulic mean depth h_0 by: $h_0 = \frac{A_0}{W}$ (the depth corresponding to an effective rectangular cross-section).

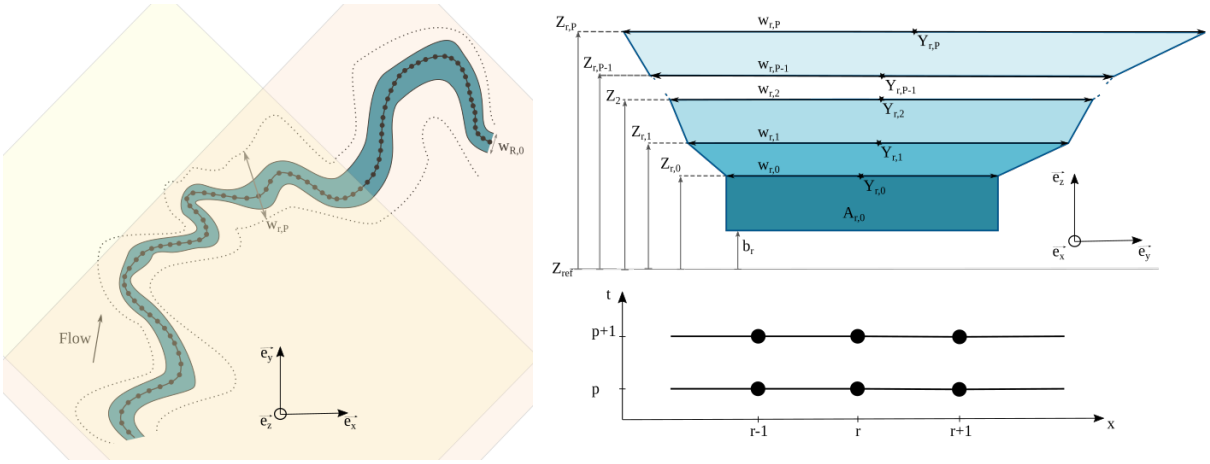

FIGURE 2.1. (Left) Schematic river plane view with satellite swaths (large colored rectangles), longitudinal grid with 1D averaged satellite measurements (black dots) along the river centerline (black line). (Right Top) Effective river cross section at reach r defined from SWOT observables $(Z_{r,p}, W_{r,p})_{R,P+1}$. (Right Bottom) Space - time stencil (r, p) (x denoting the curvilinear abscissa along the river centerline defined at low flow by $Y_{r,0}$, $\forall r$ with $Y_{r,p} \forall r, \forall p$ being the middle of each reach (observed) cross sectional width).

3. Variational Data Assimilation (VDA) algorithm

Given the WS measurements, the inverse problem consists to estimate the "input parameters" of the flow model that is : the inflow discharge, the friction coefficient and the bathymetry. The discrete unknown parameter reads:

$$c = (Q_{in,0},\ ...,\ Q_{in,P};\ b_1,\ ...,\ b_R;\ \alpha,\ \beta)^T \tag{3.1}$$

With $Q_{in,p}$, $p \in [0..P]$ the inflow discharge value at instant p, α and β roughness law parameters see (2.2), and b_r, $r \in [1..R]$, the bed elevation at reach r, see Fig. 2.1. Since the relation between the elevation Z and the wet area S (see the river description section) defines a bijection function, measuring Z is equivalent to measure S. We define the cost function:

$$j(c) = j_{obs}(c) + \gamma\, j_{reg}(c) \tag{3.2}$$

The coefficient γ is a weight coefficient, $\gamma > 0$. The term $j_{obs}(c)$ measures the misfit between the observations and the model output:

$$j_{obs}(c) = \frac{1}{2} \left\| (Z(\mathrm{c}) - Z_{obs}) \right\|_N^2 \tag{3.3}$$

with the $N-$norm defined from an a-priori covariance operator; N is a positive define matrix, $\| \cdot \|_N = \| N^{1/2} \cdot \|_2$. The elevation Z depends on c through the model (2.1); this is an optimal control problem of the (forward) model (2.1). Assuming uncorrelated observations, N is simply a diagonal matrix $N = diag(\sigma_Z)$ with σ_Z the a-priori observation error on Z_{obs}. The term $j_{reg}(c)$ is a regularization term; it is detailed later. The inverse problem reads as the optimization problem : $c^* = \mathrm{argmin\ j}(c)$. It is classically solved by a Quasi-Newton descent algorithm, here the L-BFGS algorithm presented in [29]. This first order method requires the computation of the cost gradient $\nabla j(c)$. This is done by introducing the adjoint model hence making possible to consider large control vector dimensions, see e.g. [43]. The adjoint code is obtained by employing the automatic differentiation tool Tapenade [33]. We refer to [48, 46, 47] for detailed know-hows and their implementation.

Regularization of the inverse problem and change of variable. The regularization term j_{reg} may be compulsory to solve this optimization problem. Indeed, the unknown "input parameter" contains three different variables, in particular the bathymetry $b(x)$ and the friction coefficient $K(h)$. Since these two variables are geometry related, the inverse problem may be ill-posed, see e.g. [25] and [38] for details on the theory of regularization of ill-posed problems. In the present case, the lack of regularization may lead to equifinality issues. Then we set: $j_{reg} = \frac{1}{2} \| b"(x) \|_2^2$. Next to solve more efficiently the optimization problem and following e.g. [44], we make the change of variable:

$$k = B^{-1/2}(\mathrm{c} - \mathrm{c}_{prior}) \tag{3.4}$$

with B a covariance matrix, c defined by (3.4) and c_{prior} a prior value (also called "background" value). The value of c_{prior} will depend on the context and the information a-priori available. The choice of B represents an important prior

information too since the computed optimal solution k^* depends on it. After this change of variable, the optimality condition reads: $B^{1/2}\nabla j(c) = 0$. That is this change of variable may me viewed as a preconditioning method, see e.g. [31, 32] for details. Then the new optimization problem to be solved reads:

$$\min_k \mathrm{J}(k) \tag{3.5}$$

with $\mathrm{J}(k) = j(c)$, j defined by (3.2) and the control vector k defined by (3.4). It contains the three variables $Q_{in}(t)$, $b(x)$, $K(h)$. These three variables are assumed to be uncorrelated, hence B is defined as a block diagonal matrix:

$$B = \begin{pmatrix} B_Q & 0 & 0 \\ 0 & B_b & 0 \\ 0 & 0 & B_K \end{pmatrix} \tag{3.6}$$

Each block $B_\square$ is defined as a covariance matrix (positive definite matrix). We set B_Q and B_b as the classical second order auto-regressive correlation matrix, see e.g. [44, 32, 63] :

$$(B_Q)_{i,j} = (\sigma_Q)^2 \exp\left(-\frac{|t_j - t_i|}{\Delta t_Q}\right) \text{ and } (B_b)_{i,j} = (\sigma_b)^2 \exp\left(-\frac{|x_j - x_i|}{L_b}\right) \tag{3.7}$$

The parameters Δt_Q and L_b are correlation scales. In the forthcoming numerical experiments we set: $\Delta t_Q = 24$ h and $L_b = 1$ km . The matrix B_K is diagonal; it is set as : $B_K = diag(\sigma_\alpha^2, \sigma_\beta^2)$. The four scalar values $\sigma_\square$ may be viewed as variances; their values are detailed later. In other words, the VDA formulation above takes into account prior hydraulic scales (the parameters Δt_Q and L_b) and error measurement amplitudes (the parameters $\sigma_\square$).

4. Low Complexity relations

In this section we derive direct and inverse low complexity relations between the key river flow features: the discharge Q, the bathymetry b (or equivalently the wet cross section A, see Section 2.2) and the friction coefficient K. The goals of these derivations are : 1) To infer a first estimation of the pairs $(K(h), A_{r,0})_R$ given prior values of Q; 2) To infer an accurate effective bathymetry $(b_r)_R$ given one (1) in-situ measurement; 3) To provide real time estimations of the discharge Q once the pair $(K(h), A_{0,r})_R$ has been estimated by the VDA algorithm.

The low complexity model derivations below are based on classical hydraulic assumptions but they are dedicated to the present altimetry context. The basic four assumptions are the following: 1) The satellite revisit frequency prevents to observe fast temporal dynamics, then at each observation time the flow can be described as a locally uniform and steady flow; then the river features are reach-averaged at the scale of the "observation pixel" that is ~200 m reach long for SWOT, cf Tab. 3. 2) At the present reach scale, the flow presents low Froude values; that is the inertial terms in the momentum equations can be neglected. 3) The rivers are wide enough to assume that the hydraulic radius $R_h \approx h$. (as already mentioned this has been numerically verified). 4) The flow does not present any lateral flux.

4.1. Discharge and bathymetry relations.

The non inertial flow equations derive from the permanent flow and low Froude flow hypothesis $Fr^2 << 1$. (Recall that $Fr^2 = uc_e^{-1}$ with $c_e = \sqrt{gh}$ the wave celerity for a rectangular cross section). Under these two assumptions, the momentum equation simplifies as the Manning-Strickler law: $Q = KAh^{2/3}\sqrt{S}$, with A the wet cross-section area and S the surface slope. In discrete form, this reads :

$$(K^{-1}Q_{r,p})^{3/5} = (A_{0,r} + \delta A_{r,p}) W_{r,p}^{-2/5} S_{r,p}^{3/10} \tag{4.1}$$

for each reach $r \in [1...R]$ and each satellite pass $p \in [0...P]$. In the forthcoming numerical results this system will be used with the friction coefficient varying in space, that is $K \equiv K_r$, or varying in time, that is $K \equiv K_p$.

Next by injecting the expression of Q above into the mass conservation equation $\partial_x Q = 0$, it follows the one-equation flow model : $\partial_x \left(KAR_h^{2/3}S^{1/2}\right) = 0$. If assuming that the roughness coefficient K is constant, this simplifies as: $\frac{\partial_x h}{h} = -\frac{3}{2}\left(\frac{\partial_x (S^{1/2})}{S^{1/2}} + \frac{\partial_x A}{A}\right)$. Given a reference depth value h_{ref} (measured at one location), the explicit expression h follows : $h(x) = h_{ref}\left(AS^{1/2}\right)_{ref}^{3/2} \cdot \left(AS^{1/2}\right)^{-3/2}(x)\ \forall x$. The accuracy of this explicit expression of h has been analyzed into details in [28, 25] when considering a single water elevation (A, S). In the present study we extend the approach to a complete set of observed surface elevations (hence leading to more robust and accurate estimations); moreover the derivations below show that the low Froude relations remain the same independently of the wet cross-section shapes.

If considering an effective wet cross-section $A = \alpha_A hW$, $\alpha_A \in [\frac{1}{2}, 1]$ then the bathymetry expression reads: $b(x) = Z(x) - C_{ref} \cdot \alpha_A^{-3/5}(x) \cdot (WS^{1/2})^{-3/5}(x)$ with $C_{ref} = h_{ref}\left(\alpha_A WS^{1/2}\right)|_{ref}^{3/5}$. Given the altimetric data $(Z, WS^{1/2})$ and the value S_{ref} at an arbitrary location x_{ref}, this explicit expression provides the effective bathymetry $b(x)$ (corresponding to the a-priori shape given by α_A). Let us define the observational term: $O_{r,p} = \left(W_{r,p}\sqrt{S_{r,p}}\right)^{-3/5}\ \forall r\, \forall p$. Then the bathymetry expression with $\alpha_A = 1$ reads in its discrete form as follows:

$$b_r + (Z_{ref,p} - b_{ref}) \cdot O_{ref,p}^{-1} \cdot O_{r,p} = Z_{r,p} \ \forall r,\ r \neq ref,\ \forall p \geq 0 \tag{4.2}$$

Let us point out that the altimetry observational term are Z and the product $WS^{1/2}$ only. In all the sequel the solution $(b_r)_r$ of (4.2) is so-called the "Low Froude bathymetry". This system (4.2) contains $(P+1) \times (R-1)$ equations (given 1 reference reach only) with R unknowns: the bathymetry vector $b = (\{b_r\}_r, b_{ref})$ $r \in [1, R], r \neq ref$. The system reads: $(A.b)_p = (F)_p \ \forall p$, with$(F_r)_p = Z_{r,p} - Z_{ref,p} O_{ref,p}^{-1} \cdot O_{r,p}$ and the $(R-1)(P+1) \times R$ matrix $(A)_p = \left[I_{(R-1 \times R-1)} | O_{ref,p}^{-1} \cdot O_{r,p} \right]$. For $P \geq 1$, A is of maximal rank excepted if the observational vectors $(O_r)_p$ are linearly dependent. (That is not the case if the considered water flow lines represent flow variations).

Remark 1. The three parameters (α_A, W, S) describe the three dimensions of the flow. Let us recall that considering a rectangular cross-section shape ($\alpha_A = 1$) or a different basic shape by setting α_A to a different value has no influence on the relation since the intrinsic quantity is the wet cross section$A$.

As presented in Section 5.1 the low complexity flow relations (4.1) and (4.2) are reasonably accurate at the altimetry space-time scales. Indeed these low complexity relations have been numerically assessed as follows. For the Po and Garonne rivers, the HecRas model[1] is employed to generate synthetic observations; next Gaussian noise with realistic variances are added, see Section 5.1. For the Sacramento river, SWOT Hydrology Simulator outputs are considered. Then these direct runs provide the considered "true" flows measurements. Next given the effective true bathymetry b and the synthetic data $(Z, WS^{1/2})$, the Manning-Strickler system (4.1) is solved and its solution is compared to the "true" one. The obtained difference between the discharge values deduced from (4.1) and the "true" values equal approximatively $\pm 7\%$, see Fig. 7.1. The obtained difference between the unobserved flow area A_0 infered from (4.2) and W_0, and the effective "true" value equal approximatively $\pm 10\%$ in ≈ 100 km long reaches, see Fig. 6.5. (We point out that this estimation presents an increasing "drift" from the reference in-situ measurement location x_{ref}. The drift is due to the non verified steady state mass equation $\partial_x Q = 0$. However the low Froude bathymetry is accurate enough if applied to a hundred km portion only (for a single measurement h_{ref}).

Remark 2. As already demonstrated in [28, 25], the low Froude assumption makes possible to separate the bathymetry effect from the friction effect *if* the friction coefficient K is constant, see (4.2). Indeed K does not appear anymore in the first order differential equation in $h(x)$ above. On the contrary, if K varies in space or depends on the depth h, like in (2.2) or in the Einstein formula, see e.g. [16], then K and b have coupled influence even at low Froude. Typically if considering the following power-law: $K(h) = K_0 \cdot (h - h_0)^\beta(x)$ with gradually varied coefficients i.e. $\partial_x K_0 \sim 0 \sim \partial_x \beta$, after calculations the depth expression reads: $[h(x) \cdot |h(x) - h_0|^{3\beta/2}] = c_0 \cdot (AS^{1/2})^{-3/2}(x)$ with $c_0 = |h_{ref} - h_0|^{3\beta/2} \cdot h_{ref} \cdot (AS^{1/2})_{ref}^{+3/2}$ (h_{ref} the reference depth value). (Note that the case K constant is recovered by setting $\beta = 0$).

Relationship with empirical laws. It may be practical to consider empirical laws such as: $Z_{r,p} = b_r + a_r {W_{r,p}}^\beta$. In other respects, (4.2) re-writes as follows: $Z_{r,p} = b_r + C_{ref,p} \cdot \alpha_{A,r}^{-3/5} \cdot (WS^{1/2})|_{r,p}^{-3/5} \forall r,\ \forall p,\ p = 0, .., P$ with $C_{ref,p} = h_{ref,p} \left(\alpha_A WS^{1/2}\right)_{ref,p}^{3/5}$. We assume constant cross section shapes *($\alpha_{A,r} = \alpha_A \ \forall r$)*. By equaling the two estimations it follows: ${W_{r,p}}^\beta \cdot (W_{r,p} S_{r,p}^{1/2})^{3/5} = a_r^{-1} \cdot h_{ref,p} \left(WS^{1/2}\right)_{ref,p}^{3/5}$ $\forall r\ \forall p$. Assuming that the flow is uniform in terms of the observational term $(WS^{1/2})$ i.e. this quantity is constant for the considered reaches, we obtain that: $W_p^\beta = a^{-1}\ h_p$; equivalently: $Z_p = b + a\ W_p^\beta$ **.** Therefore the low Froude estimation (4.2) contains empirical laws of the form indicated above. Given beta and time series of WS elevation and width this relation allows to infer an effective river bed elevation as suggested by [9] with $\beta = 2$. Such law could be defined in function of hydraulic geometry knowledge, see e.g. [42]. The relationship along a reach between hydraulic geometry coefficients [30] could also be investigated in the light of geomorphological variability.

Remark 3. Given a set of WS measurements $(Z_{r,p}, W_{r,p})_{R,P+1}$, given an effective low-flow bathymetry $A_{.0}$ (hence the effective wet sections $A_{r,p} = A_{r,0} + \delta A_{r,p}$ $\forall r \in [1..R]$), the inference of the *ratio* $Q_{r,p}/K_{r,p}$ is possible from the Manning-Strickler equation for all observed reach r and for all overpass p. As a consequence if considering this equation only, the resulting error on Q is proportional to the a-prior uncertainty on K^{-1}, and reciprocally.

4.2. **Inferences of the bathymetry-roughness pairs $(K_{r,p},\ A_{r,0})_r$ and real-time estimations of Q.** Given two overpasses ($P = 1$), (4.1) is over-determined hence has an unique solution in the least-square sense. Moreover the numerical results demonstrate that this solution is accurate enough to define a good "first guess" of the VDA process presented in the following section (choose preferably 2 flow profiles with significant variations). On the contrary to the VDA process, the low complexity equations derived below are extremely simple to implement and can be performed in real-time. That makes these relations very interesting for few reasons depending on the context, in particular if combined with VDA computations, see the numerical results and analysis in next sections.

[1] http://www.hec.usace.army.mil/software/hec-ras

4.2.1. *Inferences from ancillary data.* Let us assume that spatially distributed values of Q are available on the river portion for each overpass $p \in [0...P]$, that is $(Q_{r,p})_{r,p}$. These values may be provided by a hydrological model or computed by the VDA algorithm presented in Section 3. Let us assume that the roughness varies both in space and time, that is $(K_{r,p})_{r,p}$. Then (4.1) reads as follows:

$$c_{r,p} \cdot K_{r,p}^{3/5} A_{r,0} + d_{r,p} \cdot K_{r,p}^{3/5} = Q_{r,p}^{3/5} \text{ for all } (r,p) \tag{4.3}$$

with $c_{r,p} = W_{r,p}^{-2/5} S_{r,p}^{3/10}$ and $d_{r,p} = c_{r,p}\, \delta A_{r,p}$. The coefficients $(c_{r,p}\ , d_{r,p})$ can be evaluated from the altimetry measurements. System (4.3) is multi-linear in $(K_{r,p}^{3/5} A_{r,0}, K_{r,p}^{3/5}, \bar{Q}_p)$. It contains $R(P+1)$ equations. It can be employed differently depending on the available information and the unknowns. If considering the full set of unknowns $(K_{r,p}^{3/5}, A_{r,0}, Q_{r,p})$, it is an underdetermined system since it has $R(2(P+1)+1)$ unknowns; therefore in this case it cannot be solved since it has an infinity of solutions.

Let us define the diagonal matrices D_c and D_d of dimensions $[R(P+1)]^2$ by: $M_c = diag\,(c_{r,p})$, $M_d = diag\,(d_{r,p})$. Let us define the vectors : $\tilde{K} = (K_{r,p}^{3/5})_{r,p} \in R^{R(P+1)}$, $A = (A_{r,0})_r, \in R^R$ and $\tilde{Q} = (Q_{r,p}^{3/5})_{r,p} \in R^{R(P+1)}$. Then (4.3) reads:

$$D_c\, Bil(\tilde{K}, A) + D_d \tilde{K} = \tilde{Q} \text{ in } R^{R(P+1)} \tag{4.4}$$

with the bilinear operator $Bil(\tilde{K}, A)_{r,p} = K_{r,p}^{3/5} A_{r,0}\ \forall r \forall p$. If $\tilde{Q}$ is given then (4.4) has $(P+2)R$ unknowns (the two vectors $\tilde{K}$ and A).

For K constant in space but varying in time (e.g. K is defined as a power law in h) then $\tilde{K} = (K_p^{3/5})_p \in R^{(P+1)}$. In this case, the $(P+1+R)$ unknowns $(K_p^{3/5}, A_{r,0})$ can be computed by solving the overdetermined bi-linear system (4.4) e.g. by employing a trusted region reflective algorithm.

For K constant in time but varying in space, $\tilde{K} = (K_r^{3/5})_r \in R^R$, the system (4.4) has $2R$ unknowns. Therefore if $P \geq 1$ (more than 2 overpasses), the solution $(K_r^{3/5}, A_{r,0})$ can be computed e.g. by a trusted region reflective algorithm.

In the case that mean values of Q only are available, that is : $\bar{Q}_p = mean_r\,(Q_{r,p})\ \forall p$. Typically, these mean values may be deduced from local databases. Then the RHS of (4.4) reads: $\bar{Q} = \Big((\bar{Q}_0^{3/5}, ..., \bar{Q}_0^{3/5}), ..., (\bar{Q}_p^{3/5} ... \bar{Q}_p^{3/5}), ..., (\bar{Q}_P^{3/5} ... \bar{Q}_P^{3/5})\Big) \in R^{R(P+1)}$. Given $\bar{Q}$, estimations of $(A_{r,0})_r$ are obtained by computing the pairs $(K_{r,p}, A_{r,0})_{r,p}$ solution of (4.4) (with the values of $(K_{r,p})$ not necessarily used). This approach is done in Section 6.2.

Remark 4. In some contexts one can have prior estimations of $Q = (Q_{r,p}) \in R^{R(P+1)}$ provided by a hydrological model for instance, see e.g. [65, 54, 62]. Then (4.4) can be solved to obtain effective unobserved wetted areas $(A_{r,0})_r$.

4.2.2. *Real time computations of Q.* It will be shown in Section 6.1that the VDA algorithm described in Section 3 provides quite accurate values of $(A_{r,0}) \in R^R$ and $(Q_{r,p}) \in R^{R(P+1)}$. These VDA computations can be hardly performed in real-time. However as already mentioned in Section 4.1 the discrete Manning-Strickler system (4.1) provides a low-complexity direct model which is quite accurate, see e.g. Fig. 7.1. Then given $(Q_{r,p}, A_{r,0})_{r,p}$ by the (non real time) VDA algorithm, the effective space-time dependent roughness coefficient $(K_{r,p})_{r,p}$ can be computed from (4.4). Next given new observations sets $(Z_r, W_r)_R$, typically satellite observations acquired after the "learning period", the corresponding discharge values Q_r can be computed in real-time simply by evaluating the Manning-Strickler equation. Such real-time estimations are presented in Section 7.

5. Test rivers and data description

5.1. **River cases and free surface observations.** The performances of the VDA algorithm and the low complexity relations previously introduced are assessed on three portion rivers . They consist in 75km of the Garonne River (France), 98km of the Po River (Italy) and 147km of the Sacramento River (California, USA), see Table 1 for details. The Po and Garonne rivers represent two orders of magnitude of discharge for a Cal/Val scenario; the nominal SWOT sampling is tested on the Sacramento River.

The SWOT-like WS observations used in the following VDA experiments consist for each river in sets of $(Z_{r,p}, W_{r,p})_{R,P+1}$. These data are generated either by adding Gaussian noise to 1D hydrodynamic model outputs sampled at $\Delta x_{obs} = 200$ m in space (Garonne and Po river cases) or by using the SWOT-HR simulator outputs averaged in space on 200 m reaches (i.e. RiverObs node average spacing, Sacramento River case). The synthetic data are as follows: $Z_{obs}(x,t) = Z_{true}(x,t) + N(0, \sigma_Z)$ with $\sigma_Z = 25$ cm corresponding to the expected magnitude of SWOT measurement errors at the present spatial scale. Also we set $\Delta t_{obs} = 1$ day, that is a frequency revisit corresponding to the calibration/validation (Cal/Val) phase period of the SWOT mission. For the Sacramento case, the observability corresponding to a nominal 21 days SWOT cycle is simulated by the SWOT-HR simulator. The whole reach is observed by SWOT (tracks number #249 and #527 respectively) at day 9 and 19 for each 21 days repeat cycle; the simulated measurement error on Z is characterized on average by a variance $\sigma_Z = 34$ cm, see Tab. 1.

Case Name	Reach Length (km)	Max. Width (m)	Avg. Slope (m/km)	Avg. Flow (m3/s)	Froude Range (-)
Garonne (US)	75	49/1,383	0.861	156	0.03-0.67
Po	98	116/5,515	0.145	1499	0.04-0.47
Sacramento	147	59/678	0.558	251	0.02-0.64

TABLE 1. Hydraulic characteristics for each case

Case Name	Hydrodynamic Model	Temporal Window	Observations Frequency	Reference
Garonne (US)	HEC-RAS	06 jan. 2010 - 06 avr. 2010	1 day	[40]
Po	HEC-RAS	01 jan. 2002 - 01 avr. 2002	1 day	[20]
Sacramento	HEC-RAS + SWOT HR	01 jan. 2009 - 27 jun. 2009	21 days	[58]

TABLE 2. Observations sources and characteristics for each case

5.2. **Classes of inverse problems for ungauged and poorly gauged rivers.** The future SWOT mission will observe worldwide rivers larger than 100 m with on average 1 to 4 temporal revisits every 21 days at mid-latitudes, see e.g. [7]. Given a river portion, the difficulty of the inverse problem previously described depends on the availability or not of ancillary data. The inversion capabilities of the algorithms and relations proposed in this article are tested on three scenarios. All scenarios are based on a set of SWOT observations consisting in a set of river surface deformations $(Z_{r,p}, W_{r,p})_{R,P+1}$ measurements. These scenarios present a decreasing complexity in the sense the first one, the most challenging, considers SWOT data only, the last one, the easiest one, considers additional informative in-situ data. For each river case these three scenarios, based on SWOT data either with Cal/Val daily revisits or a nominal SWOT orbit, see Section 5.1 and Table 2, depend on the availability or not of in-situ / ancillary data:

(1) Only SWOT observations are available, which corresponds to the most challenging inverse problem on ungauged rivers.
(2) Only SWOT observations and multi-temporal priors on discharge are available from worldwide hydrological models, which correspond to ungauged or poorly gauged rivers. An effective bathymetry can be inferred thanks to the low complexity system (cf. next paragraph)
(3) SWOT observations and one in-situ measurement of bathymetry (b_{ref}) are available, hence an effective bathymetry can be infered (cf. next paragraph).

For all scenarios and river cases an available worldwide river database - the SWOT a-priori river database [2, 17, 1] in construction - contains (among other variables coming from databases described in references) at least one discharge value (inter-annual average value of discharge modeled with a large scale water balance model or estimated from ancillary hydrological databases) and one roughness estimate. Given the $R \times (P+1)$ WS observations, the complete control vector c, see Eqn (3.1, formed by $(P+4R+2)$ unknowns is computed by VDA. It is formed by $(P+1)$ unknown discharges, $4R$ unknown river bed elevations and a roughness parameterization depending on forward model state and 2 parameters assumed constant in space.

5.3. **First guess computation and performance assessment criteria.** In view of to be as realistic as possible, first guesses of the VDA process are infered from available worldwide databases and/or hydrological models. Recall that for many river portions worldwide, in-situ measurements will not be accessible or even do not exist. First guess values $c^{(0)} = \left(Q^{(0)}_{in,0}, ..., Q^{(0)}_{in,P}; b^{(0)}_1, ..., b^{(0)}_R; \alpha^{(0)}, \beta^{(0)}\right)^T$ of the parameter vector, see (3.1) and (3.4), is obtained as follows:

- A constant prior on discharge $Q^{(0)}_{in,p} = Q_{MAF}, \forall p \in [0...P]$, is obtained by retrieving Mean Annual Flow (MAF) either from the SWOT a-priori river database [2, 17, 1] or from the global Water Balance Model [65]. So far, the WBM discharge is preferred in the SWOT discharge community as a reference**.**
- A constant prior on Strickler roughness coefficient $K^{(0)}$ is estimated from the SWOT a-priori river database under construction. The $K^{(0)}$ values in the present case are 25, 33 and 25 respectively for the Garonne, Po, and Sacramento rivers (i.e. it the $\alpha^{(0)}$ values with $\beta^{(0)} = 1$, see (2.2)).
- A prior on the unobserved low flow $b^{(0)}$ (or equivalently the low flow cross sectional areas $(A_{r,0})_r$ assuming a shape and knowing the low flow WS widths $(W_{r,0})_r$, see Section 4.2) can be obtained by the following three methods (Table 3).
  - *"Manning"* - the unobserved low flow bathymetry $b^{(0)}$ is obtained by inverting the Manning equation (4.1) applied to a single flow line with $K^{(0)}$ and Q_{WBM} constant in space and time,
  - *"Manning-multi"* - low flow bathymetry $b^{(0)}$ is obtained by inverting equation (4.3) with numerous flow lines that represent a large range of flow regimes and variabilities on the studied river portion. In that

Experiment	River	$b^{(0)}$	Δx_{obs}	Δt_{obs}	$\sigma_Z^{perturb}$	σ_Z	σ_Q	σ_{α_K}	σ_{β_K}	σ_b
A.1	Garonne	Manning	200 m	1 day	0	25 cm	15 m3/s	0.5	0.01	25 cm
A.2	Garonne	Manning-multi	200 m	1 day	0	25 cm	15 m3/s	0.5	0.01	25 cm
A.3	Garonne	LowFroude	200 m	1 day	0	25 cm	15 m3/s	0.5	0.01	25 cm
A.4	Garonne	Manning	200 m	1 day	25 cm	25 cm	15 m3/s	0.5	0.01	25 cm
A.5	Garonne	Manning-multi	200 m	1 day	25 cm	25 cm	15 m3/s	0.5	0.01	25 cm
A.6	Garonne	LowFroude	200 m	1 day	25 cm	25 cm	15 m3/s	0.5	0.01	25 cm
B.1	Po	Manning	200 m	1 day	0	25 cm	71 m3/s	0.5	0.01	25 cm
B.2	Po	Manning-multi	200 m	1 day	0	25 cm	71 m3/s	0.5	0.01	25 cm
B.3	Po	LowFroude	200 m	1 day	0	25 cm	71 m3/s	0.5	0.01	25 cm
B.4	Po	Manning	200 m	1 day	25 cm	25 cm	71 m3/s	0.5	0.01	25 cm
B.5	Po	Manning-multi	200 m	1 day	25 cm	25 cm	71 m3/s	0.5	0.01	25 cm
B.6	Po	LowFroude	200 m	1 day	25 cm	25 cm	71 m3/s	0.5	0.01	25 cm
C.1	Sacramento	Manning	200m	21 days*	0	25 cm	20 m3/s	0.5	0.01	25 cm
C.2	Sacramento	LowFroude	200m	21 days*	0	25 cm	20 m3/s	0.5	0.01	25 cm
C.3	Sacramento	Manning	200m	21 days*	34 cm	25 cm	20 m3/s	0.5	0.01	25 cm
C.4	Sacramento	LowFroude	200m	21 days*	34 cm	25 cm	20 m3/s	0.5	0.01	25 cm

TABLE 3. Summary of experiments (*:two overpasses at days 9 and 19 every 21 days repeat period)

case, flow lines can be grouped by deciles and put in correspondence with deciles of discharge from the worldwide available WBM model.

– *"LowFroude"* - In the case of one (1) bathymetry point is available, an effective bathymetry is derived from WS observables and the low Froude equation (4.2).

Remark 5. It is important to point out that if $b^{(0)}$ is estimated from the simple one-value Manning-Strickler relation, this first crucial estimation of the bathymetry is highly sensitive to any error made on the a-priori estimation of $(Q^{(0)}, K^{(0)})$.

These three scenarios are tested on all river cases, either with perfect or noisy observations, except for the Sacramento River were the second scenario cannot be computed. Indeed the small number of overpasses (17) is not sufficient to determine flow regimes an thus statistically relate observations with databases.

The cost functions used to evaluate the performance of inversions at assimilation times consists in classical $RMSE = \sqrt{\frac{\sum_{t=1}^{n}(Q_t^{est}-Q_t^{true})^2}{n}}$ and relative RMSE $rRMSE = \sqrt{\frac{1}{n}\sum_{t=1}^{n}\left(\frac{Q_t^{est}-Q_t^{true}}{Q_t^{true}}\right)^2}$ where Q_{in}^{est} (resp. Q_{in}^{true}) is the estimated (resp. observed) inflow discharge of size n in time.

6. Hydraulic inversions from long time series of water elevation measurements

This section presents the inference of the complete control vector of the 1D Saint-Venant river flow model, which contains discharges, bathymetry and roughness. It is infered by assimilating the SWOT-like WS observables, see Section 5.1 and Table 2, into the hydrodynamic model (2.1) using the VDA method described in Section 3. Three scenarios of decreasing complexity are tested from the very challenging one with SWOT data and worldwide databases only and next for increasing ancillary river data including in-situ data for the last scenario, see Section 5.2. The identifiability of river parameters is tested on the three portion rivers (see Section 5.1) using the open source DassFlow-1D software [47].

6.1. **Hydraulic inferences from SWOT data on ungauged rivers.** In this section a real-like SWOT data context is considered; the hydraulic optimization problem solved by VDA is started from a prior control vector $c^{(0)}$ infered from worldwide available databases. The latter are used to infer a prior roughness $K^{(0)}$ and bathymetry $b^{(0)}$ (*"Manning"* or *"Manning-multi"*) as explained above (Section 5.1). For each of the three river cases, a set of water elevations and width $(W, Z)_{R,P+1}$ measurements is considered for R reaches and $(P+1)$ revisits. The complete set of river parameters $c = (Q_{in,0}, ..., Q_{in,P}; b_1, ..., b_R; \alpha, \beta)^T$ is sought by minimizing (3.5), inverse problem described in Section 3.

Two SWOT temporal samplings are considered, corresponding to the two successive phases of the future SWOT mission. First a Cal/Val scenario with daily observations on the Po and Garonne Rivers representing two orders of magnitude of discharge; second a real SWOT scenario on the Sacramento River are investigated with 2 observations for each 21 days period. The performances on river parameters inference, with various combinations of first guesses and observational sparsities are summed up in Table 4. For all experiments, over fitting the data is avoided by applying Morozov's principle, see e.g. [38] and references therein. Due to the regularization and the covariance operators introduced in the VDA formulation, Section 3, the iterative process is relatively fast and robust, see the good performances in Table 4. For the 16 inverse computations (10 ungauged cases) performed, the first guess values are systematically greatly improved.

6.1.1. *SWOT Cal/Val inferences: the Po and Garonne rivers.* The inflow discharge, bathymetry and roughness infered by VDA on the Garonne and Po Rivers are shown in purple on Fig. 6.1 (SWOT Cal/Val scenarios A.4 and B.4). For each river the daily inflow hydrograph over 90 days (green curve) is satisfactorily retrieved with $rRMSE_Q = 24.3\%$ on the Po River the and $rRMSE_Q = 9\%$ on the Garonne River at assimilation points (corresponding to observation points) - 8.5% and 4.8% respectively with perfect observations. Both the discharge and roughness inference are accurate despite the daily measurement errors. The estimated bathymetry $b_{1..R}$, see Table 4 and purple curves on Fig. 6.4, is improved by the VDA process on the Garonne River (prior $RMSE_{b^{(0)}} = 0.39$ decreases to $RMSE_b = 0.31$) ; it remains close to the first guess in the Po River case. Let us recall that the roughness parameter K is model-equations-geometry dependent; its calibrated value compensate various modeling errors.

For both rivers considered as ungauged i.e. with prior $c^{(0)}$ defined from databases (scenarios A4,5 ; B4,5 and A1,2 ; B1,2 with perfect observations, Table 4), the inference of discharge remains robust and accurate. Most of the identification errors are absorbed by the roughness coefficient. Despite the improvement of robustness of the present enriched VDA method, some equifinality may remain between the bathymetry and the roughness. Indeed, on the Po River while discharge is very well retrieved, neither the bathymetry nor the roughness are significantly improved by the VDA process. An infinity of roughness and bathymetry values (embedded in the friction source term of the Saint-Venant equations) can mathematically produce the correct discharge given a flow stage. However the optimal value of the pair $(b(x), K)$, in the sense of the optimization problem (3.5), can be refined thanks to the low complexity relations presented in Section 7, see Table 4.

The "*Manning*" method has been performed using the WBM discharge [65] and the discharge in the SWOT a-priori river database [2, 17, 1]. Recall that the "*Manning*" method to determine the prior value of $b^{(0)}$ is based on a single pair value $(Q^{(0)}, K^{(0)})$, therefore it is highly sensitive to any error, see Remark 5. To illustrate this, the cases A.1, A.4, B.1, B.4, C.1, C.3 have been performed from a quite rough prior values (provided by WBM) and from quite excellent ones (provided by the SWOT a-priori river database). The results are presented in Table 4 for these 6 cases with the obtained values from WBM and those from other priors are in parenthesis "(resp.)". The results obtained for these 6 experiments show that rough priors in discharge lead to poor estimations of the discharges. For the A.1 case (resp. A.4 case), using the WBM inflow prior leads to $rRMSE_Q = 52.5\,\%$, and $rRMSE_Q = 4.8\,\%$ using a correct inflow prior (resp. $rRMSE_Q = 61.0\,\%$ and $rRMSE_Q = 9.0\,\%$). For the B.1 case (resp. B.4 case), using the WBM inflow prior leads to $rRMSE_Q = 23.5\,\%$, and $rRMSE_Q = 8.5\,\%$ using a correct inflow prior (resp. $rRMSE_Q = 41.5\,\%$ and $rRMSE_Q = 24.8\,\%$). Finally for the C.1 case (resp. C.3 case), using the WBM inflow prior leads to $rRMSE_Q = 75.9\,\%$, and $rRMSE_Q = 11.5\,\%$ using a correct inflow prior (resp. $rRMSE_Q = 98.7\,\%$ and $rRMSE_Q = 19.3\,\%$). These results show that the estimations are highly sensitive to the accuracy of the inflow prior if using the simple *"Manning"* method. On the contrary, is using multiple discharges values (here from the GRDC database) that is using the *"Manning-Multi"* method, these estimations are much more robust.

6.1.2. *SWOT inferences and identifiability map (Sacramento River case).* The discharge inference capabilities depend on the space-time sampling of the observations and on the flow dynamics. An instructive reading of the inverse problem

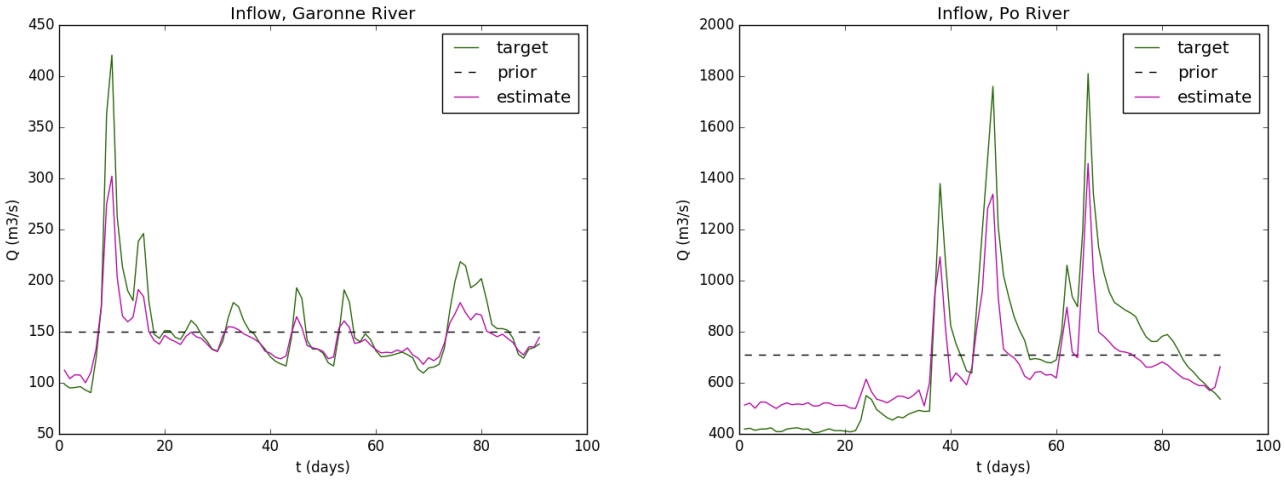

FIGURE 6.1. Inflow discharge (true=target, prior, infered=estimate) with daily SWOT-like observations. (Left) Garonne River Case A.3. (Right) Case B.3

stiffness can be obtained by plotting the "identifiability map" introduced in [11]. The identifiability map represents in the (x,t) plane the complete information : the "space-time windows" observed by SWOT, the hydrodynamic wave propagation (1D Saint-Venant model in fluvial regime) and the misfit to the "local equilibrium" (local misfit between the steady state uniform flow and the dynamics flow), see [11] for more details. This preliminary analysis makes possible to roughly estimate the inflow time intervals that can be quantified by VDA (the inflow discharge values arise from these observed "space-time windows"). This quantitative reading of the inverse problem is instructive since it makes possible to roughly estimate if the sought information has been observed or not. In the present case (Sacramento River case), the reach of 147 km long is completely observed by two SWOT tracks respectively at day 9 and 19 for each 21 days repeat period.

Fig. 6.2. Due to the observation layover there are few unobserved zones for the second SWOT pass #527, for example at $x = 80$ km and $t = 19, 40, 61$ days. Given the WS observation of each reach at a given time, on Fig. 6.2 purple dots at the upstream BC represent the foot of each hydraulic characteristics - the upward hydraulic information propagation. Then, the identifiability of $Q_{in}(t)$ appears to be possible on time windows of ∼3 days (∼2 days for the flood peak recession at day 51) before observation times.

Another information, the "equilibrium misfit", is represented on this map and it highlights where and when the flow is not locally steady and uniform. The magnitude of this equilibrium misfit tends to increase when a flood wave is traveling through the domain as shown by the observation at day 51, and day 61 corresponding to another peak entering the studied domain, figures 6.2 and 6.3. The map indicates that the WS deformations due to the flood peak between day 51 and 61 have not been observed. Moreover the mean estimated upward information propagation time is of 72h.

Consequently, from this analysis we define 3 assimilation points every 12h, hence corresponding to half the mean propagation time, before observations at days 51 and 61. Those observations may contain information respectively on the first flood peak recession and the third flood peak rising. The mean estimated upward propagation time is 36h (estimation coming from "observable times", which are represented with vertical purple dots on the right side of the figure). Since these "observable times" are computed a-posteriori and using an estimation of the wave speeds, we dismissed the extrema values (we retain 70% of the values).

6.1.3. *SWOT inferences (Sacramento river).* The accuracy and the robustness of the algorithms proposed in this study are demonstrated on a real SWOT scenario, that is with relatively sparse observations in time compared to the inflow hydrograph frequencies. The identifiability maps provides some crucial information to define assimilation points before SWOT observation points. Indeed WS deformations observed at a given time over a river domain are caused by past variations of the sought inflow hydrograph at the upstream of the river domain. The inflow discharge, bathymetry and roughness infered by VDA on the Sacramento River are shown respectively on Fig. 6.3 (Left) and Table 4. As expected following the analysis made above with identifiability maps, the discharge identification is accurate at each observation time and for the 3 points preceding observed flood peaks at $t = 51$ and 61 days. It is worth to notice that a a basic approach consisting in infering discharge at observation times only would lead to a less accurate hydrograph inference as shown in Fig. 6.3 (Right). Recall that the flood peak between days 51 and 61 is not retrieved since the analysis above shows that the peak effects have not been observed.

Following [11], the identifiability index $I_{ident} = \frac{T_{wave}}{\Delta t_{obs}}$ of the river case is evaluated for a wave propagation time of about $72h$ (with $\Delta t_{obs} \sim 10$ days), it gives $I_{ident} \sim 0.3$, that is a relatively low identifiability index. Interestingly,

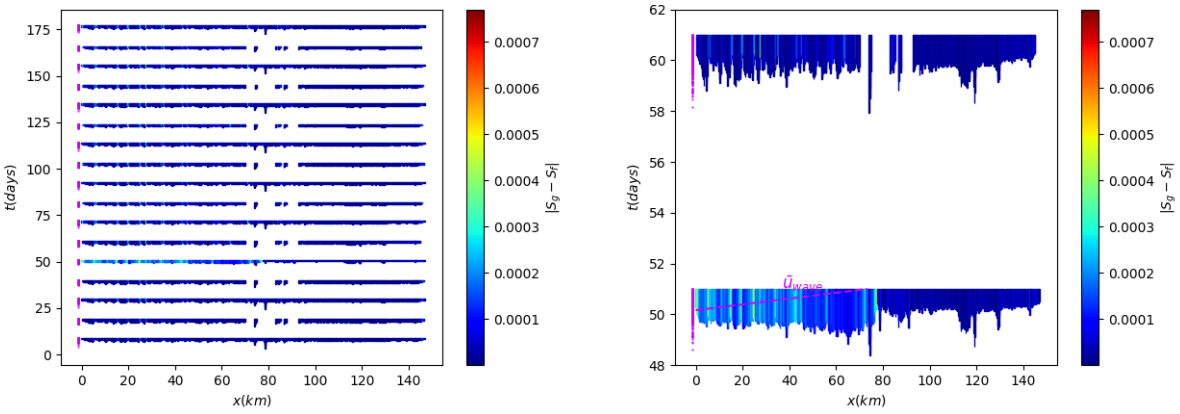

FIGURE 6.2. Identifiability map: overview in the (x,t)-plane of the inverse problem features: observables, hydraulic wave speed (and "equilibrium misfit" being absolute value of the source term in the Saint-Venant equation, color bar). For each observation of the domain in time, the vertical spreading corresponds to the time $\frac{\alpha}{u}\Delta x$ necessary for the upstream wave to cross an observed cell of size Δx; α is simply a dilatation factor for a sake of readibility. . (Up) The complete (x,t)-plane. (Down) Zoom on the most varying time intervall.

even with this low value low identifiability, the inference of discharge is accurate at observation points but also at the identification times before flood observations defined thanks to identifiability maps.

Finally we point out that the infered discharge is accurate while the bathymetry and roughness need to be refined using other information or equations; this is done in next section using the low complexity relations presented in Section 4. In other respect, this test case highlights the huge importance of using an unsteady model (1D SW here) in order to be able to simulate nonlinear flow dynamics between (sparse and unevenly spaced) assimilation points.

6.2. **Inferences from SWOT and one (1) in-situ bathymetry point with the low-Froude model.** Many rivers worldwide are not ungauged; then this section assesses the benefit of using an additional in-situ bathymetry data for defining a first guess of the control vector $c^{(0)}$ in the VDA process (case *"LowFroude"* Section 5.3).

6.2.1. *Bathymetry estimations.* Infering a reliable prior bathymetry may be an important step before the iterative VDA process. Recall that the control vector c is composed by the upstream discharge , the bathymetry and the roughness, see (3.1). The different alternatives presented in Section 5.3 for estimating low flow bathymetry are tested on the three river cases, Fig. 6.4. Each method gives fairly good estimations of $(b_r)_{1..R}$ (represented here as b^* the bed elevation b minus an average bathymetry trend). For each river, unsurprisingly, the best estimate is given by the low Froude approach, Eqn (4.2) requiring one (1) in-situ point. Using the approaches based on the Manning equation and one flow line ($b^{(0)}$ *"Manning"*, Eqn (4.1)) leads to a shift of the infered prior bathymetry (Po and Sacramento rivers) whereas it is avoided if using the low complexity approach involving multiple flow lines better sampling flow regimes ($b^{(0)}$ *"Manning-multi"*, Eqn (4.3)).

In the Sacramento river case, a drift (increasing error in space) appears in the *"LowFroude"* bathymetry for nodes far from the reference point. Indeed if the basic hypothesis $\partial_x Q = 0$ of *"LowFroude"* model is not satisfied (that is an unsteady flow), such a drift appears due to the nature of the differential equation (a first order differential equation), see [25] for a detailed investigation. In order to avoid this drift, a segmentation of the river into two zones is performed and two reference bathymetry points are used for the *"LowFroude"* bathymetry prior estimation, Fig. 6.4 (Bottom Right).

6.2.2. *VDA inferences from prior bathymetry estimations.* In this paragraph, the impact of bathymetry prior on the control vector c, Eqn (3.1), infered by VDA is detailed. For each river, the infered inflow hydrograph starting from a "LowFroude bathymetry" prior (see Section 6.2.1 and Fig. 6.4) is shown on Fig. 6.5. For the Sacramento river, both VDA runs C.3 and C.4, performed either with *"Manning"* or *"LowFroude"* bathymetry priors, result in comparable errors ($rRMSE_Q \sim 20\%$); the bathymetry is slightly degraded but the inversion remains robust. For the Garonne River the inversions performed with the 3 different bathymetry first guesses result in comparable errors ($rRMSE_Q = 8.5\%$ and 9.1%, runs C.3 and C.4). The finest bathymetry infered by VDA results from the use of *"Manning"* or *"LowFroude"* bathymetry first guesses - that provide fairly accurate priors in that case. For the Po River, using a *"LowFroude"* bathymetry results in the best error ($rRMSE_Q = 18.3\%$, run B.6) compared to other bathymetry first guesses (runs B.4 and B.5). This bathymetry is also slightly improved by the VDA process.

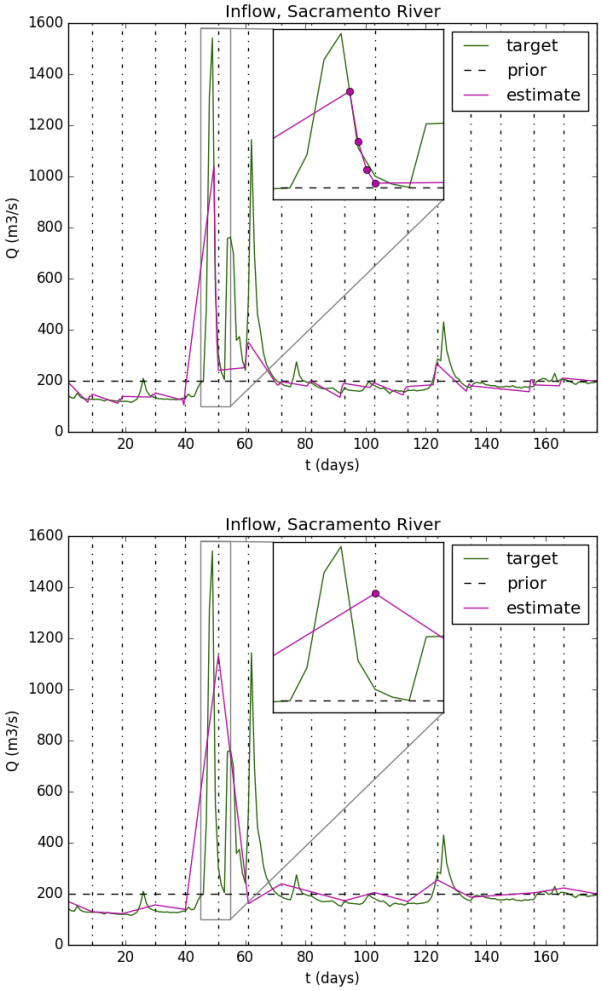

FIGURE 6.3. Inflow discharge (target=true, prior and infered=estimate with SWOT-HR observations), Sacramento River. Computations with $N = 4$ assimilation points every ($0h$,$12h$,$24h$,$36h$) before observation times (Left) or at observation times only (Right).

As shown in Section 6.1.1 the accuracy of the infered triplet $(Q(t), b(x), K)$ with the present algorithms depend on the accuracy of the prior estimations; however due to the change of variable and covariance operators introduced in the VDA formulation (equivalently a regularization term), see Section 3, the triplet inference is robust (in terms of convergence and computed optimal solution).

7. Real-time estimations of Q given $(A_{r,0}, K)$

As previously shown, robust and accurate estimations of the discharge are obtained using the present inversion algorithms (VDA process, prior strategies and Saint-Venant's equations) and a more or less large SWOT observations set. It is highly advisable to perform theses inversions on a complete hydrological cycle (i.e. a one year complete set of flow regimes) since they provide the optimal values in a least-square sense (with respect to the Saint-Venant equations and the observations sampling) of the "pair" bathymetry $b(x)$ and the roughness coefficient K (see e.g. [10, 46]for detailed explanations of the VDA solutions meaning). However it is important to recall that K (constant parameter or not) is fully model dependent. Moreover the iterative VDA process cannot be performed in real-time (with respect to the satellite data acquirements) yet. Then, once the VDA based inversion process has been performed on a complete SWOT observation set (typically a complete hydrological year), somehow the learning period, the low-complexity relations presented in Section 4 can be re-calibrated; hence making possible to infer the inflow discharge in real-time (i.e. as soon as new SWOT measurements are acquired). The re-calibration of the roughness coefficient is done following one of these two methods :

- $K_r = mean_p(K_{r,p})$, hence K is constant in time by time intervals. The mean is computed on a subset of the WS observations eg by considering the 2^{nd} - 8^{th} deciles of the flow profiles (here 20 overpasses) since this corresponds to relatively wide and representative range of flow regimes without the extremes. We compute $K_{r,p}$ by inverting Eqn (4.1); next the temporal averaging above provides the spatially distributed roughness coefficient K_r.

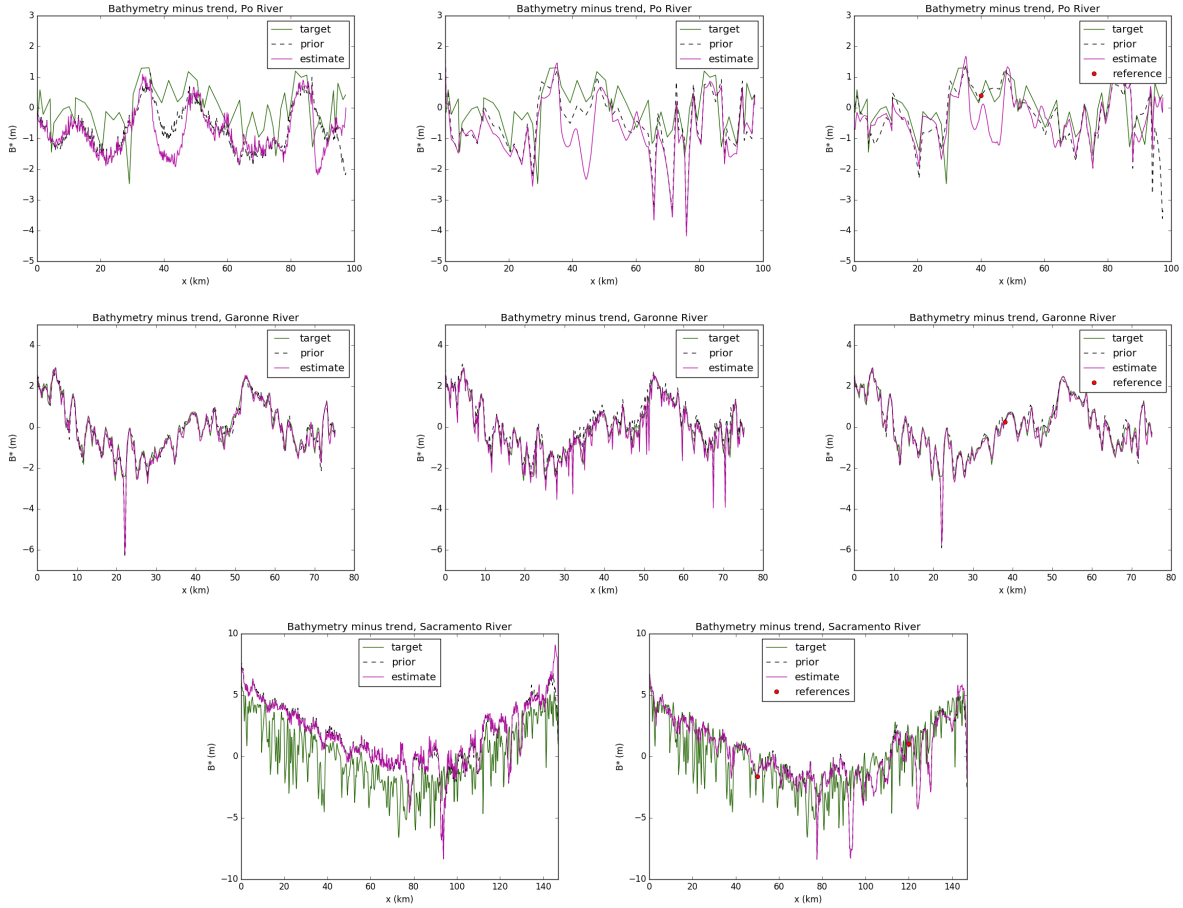

FIGURE 6.4. True and infered bathymetry trend $(b^*)_{1..R}$ compared to prior bathymetry estimations, noisy observations (Section 5.3): (Left) "Manning". (Top and Middle Center) "Manning-multi". (Right) "LowFroude".

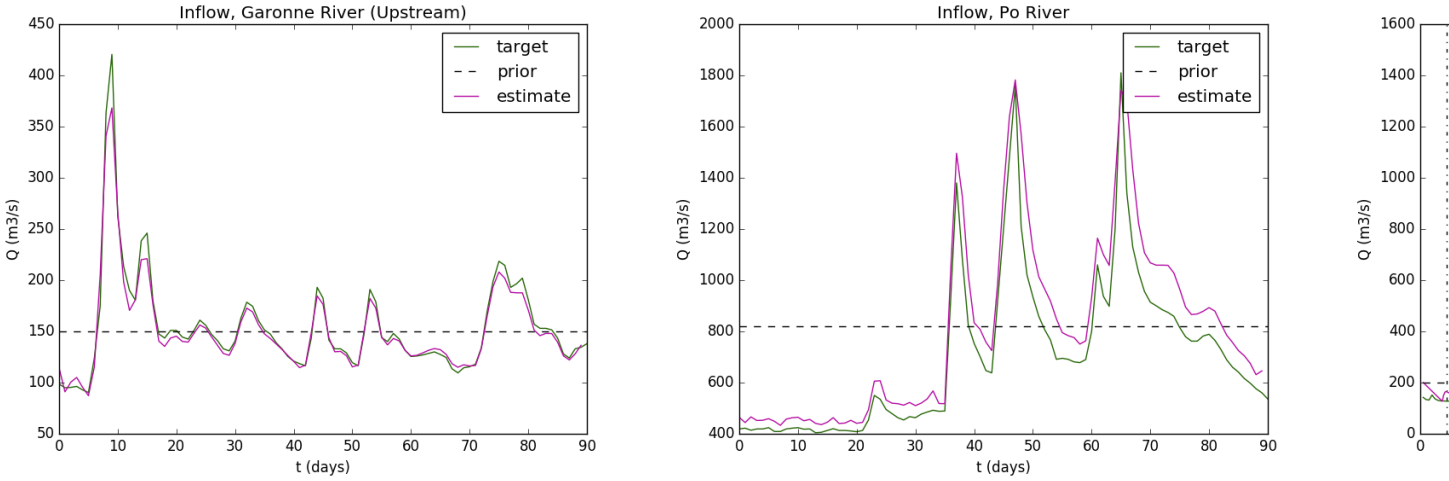

FIGURE 6.5. Infered inflow discharge with the bathymetry priors infered using the Low-Froude model and one (1) in-situ point ($b^{(0)}$ "LowFroude"). Daily SWOT-like observations (noise $\sigma_Z = 0.25$) (Top, Middle) and SWOT-HR observations (Bottom).

- $K_{r,p} = K_r(h_{r,p}) = \alpha_r {h_{r,p}}^{\beta_r}$, with α_r and β_r defined for each river reach, hence distributed in time and space. It is estimated from the low flow bathymetry $(b_r)_{1..R}$ infered by VDA, hence providing the water depth $h_{r,p}$. Note that the hydraulic parameters are infered on the 1D model grid which is finer than the observation grid, hence the inversion outputs are aggregated (spatial average) on each reach r, $r \in [1..R]$. Next, $h_{r,p} = (Z_{r,p} - b_r)$, and for each reach r a simple least-square fitting with respect to (α_r, β_r) provides $K_{r,p} = \alpha_r {h_{r,p}}^{\beta_r}$.

Case	River	σ_Z^{obs}	b_{prior}	$RMSE_{b^{(0)}}$ (m)	$RMSE_Q$ (m^3/s)	$rRMSE_Q$ (%)	$RMSE_b$ (m)
A.1	Garonne	0	Manning	0.71 (resp. 0.18)	76.9 (resp. 8.85)	52.5 (resp. 4.8)	0.69 (resp. 0.27)
A.2	Garonne	0	Manning-multi	0.17	10.0	4.2	0.16
A.3	Garonne	0	LowFroude	0.16	11.9	5.2	0.22
A.4	Garonne	25 cm	Manning	0.59 (resp. 0.39)	100.4 (resp. 22.1)	61.0 (resp. 9.0)	0.45 (resp. 0.31)
A.5	Garonne	25 cm	Manning-multi	0.42	17.9	8.5	0.38
A.6	Garonne	25 cm	LowFroude	0.35	19.4	9.1	0.27
B.1	Po	0	Manning	0.94 (resp. 0.61)	117.7 (resp. 83.9)	23.5 (resp. 8.5)	1.09 (resp. 0.75)
B.2	Po	0	Manning-multi	0.73	91.2	10.2	0.88
B.3	Po	0	LowFroude	0.48	76.4	7.8	0.45
B.4	Po	25 cm	Manning	0.97 (resp. 0.92)	215.2 (resp. 185.9)	41.5 (resp. 24.8)	1.19 (resp. 1.04)
B.5	Po	25 cm	Manning-multi	0.83	183.7	24.3	1.07
B.6	Po	25 cm	LowFroude	0.64	144.8	18.3	0.60
C.1	Sacramento	0	Manning	1.61 (resp. 2.29)	139.2 (resp. 30.1)	75.9 (resp. 11.5)	1.84 (resp. 2.33)
C.2	Sacramento	0	LowFroude	1.95	54.5	15.9	2.01
C.3	Sacramento	34 cm	Manning	2.25 (resp. 2.45)	176.1 (resp. 124.7)	98.7 (resp. 19.3)	2.28 (resp. 2.49)
C.4	Sacramento	34 cm	LowFroude	1.84	141.2	20.2	1.82

TABLE 4. Scores of the inversions performed from different priors defining the bathymetry first guess $b^{(0)}$, see Section 5.3.

Given these re-calibrated roughness coefficients $(K_r)_{1..R}$, the discharge is computed using simply the Manning equation (4.1) from the newly acquired SWOT like observations. The obtained values in the case of the Po and Garonne Rivers are plotted on Fig. 7.1 for all available flow lines. (Note that WS slopes are obtained by downstream finite difference from observed WS elevation between two observed points). For both rivers, using a roughness coefficient K_r constant in time gives the best results. The resulting errors are $rRMSE_Q = 6.3\%$ for the Garonne River and $rRMSE_Q = 10.6\%$ for the Po River. The second method to re-calibrate the roughness $K_{r,p}$ provides good results too; the errors are $rRMSE_Q = 9.1\%$ for the Garonne River and $rRMSE_Q = 25.3\%$ for the Po River. Note that these performances are evaluated at all observation times but for all discharges in space contrarily to the discharge infered by VDA (see Section 6) upstream of the river domain, i.e. only for $r = 0$.

The spread of discharges for the highest flow regimes could be reduced with a more complex friction law accounting for compound channel head loss. However, the proposed approach based on the present low complexity relations (after a re-calibration of the roughness coefficient as presented above) appears very promising to perform the discharge in real-time, that is in an operational way.

8. Conclusion

This study proposes and assess a new computational hierarchical strategy to infer the discharge and the river key features (effective bathymetry with the corresponding roughness coefficients) from WS altimetry measurements only; more specifically the forthcoming SWOT swath altimetry observations. The inverse algorithm is based on a combination of an advanced Variational Data Assimilation (VDA) formulation applied to the Saint-Venant equations (1D shallow-water) and original forward-inverse low complexity algebraic systems (permanent low-Froude flow laws). The cross sections are effective since they are defined from the satellite measurements (trapezium super-impositions). If no prior information is available (that is the case of numerous ungauged rivers in the world), the inverse process remains robust and accurate providing the key triplet $Q(t)$, $b(x)$ and $K(h)$. The VDA process applied to the hydrodynamic model propagating in space-time the informative content of the WS measurements. The original low complexity systems are central for few reasons. Firstly they make possible to exploit in a physically consistent manner (local or global) databases in view to define the first guesses (prior information) of the iterative VDA process. Secondly they make possible to compute in real-time the discharge past the "learning period" by the VDA process (i.e. past the assimilation of a complete hydrological year). The advanced formulation of the VDA process takes into account a-priori scale dependency and a-priori error measurement amplitudes. On the three considered river portions of ~ 100 km long, that is presenting low identifiability indexes hence challenging inverse problems, see [11], all the inferences are accurate for the two scenarios of observation: 1) the SWOT Cal-Val orbit with ~ 1 day period (or any equivalent multiple-sensor measurements) ; 2) SWOT like data with 21 days period (with 1 to 4 passes at mid-latitudes). Preliminary analysis based on the identifiability maps introduced in [11] help to define adequate time grids for the identified discharge. The estimation of the discharge $Q(t)$ is always accurate whatever the configuration, ungauged river portion or not (that is with available database values). In the case of lack of good prior information (ungauged river or too approximative database values), the present original low complexity systems improve significantly the accuracy of the infered bathymetry $b(x)$ compared to the use of the "simple" Manning-Strickler equation (the latter being much more sensitive to any a-priori errors). However the infered bathymetry may still be dependent on the

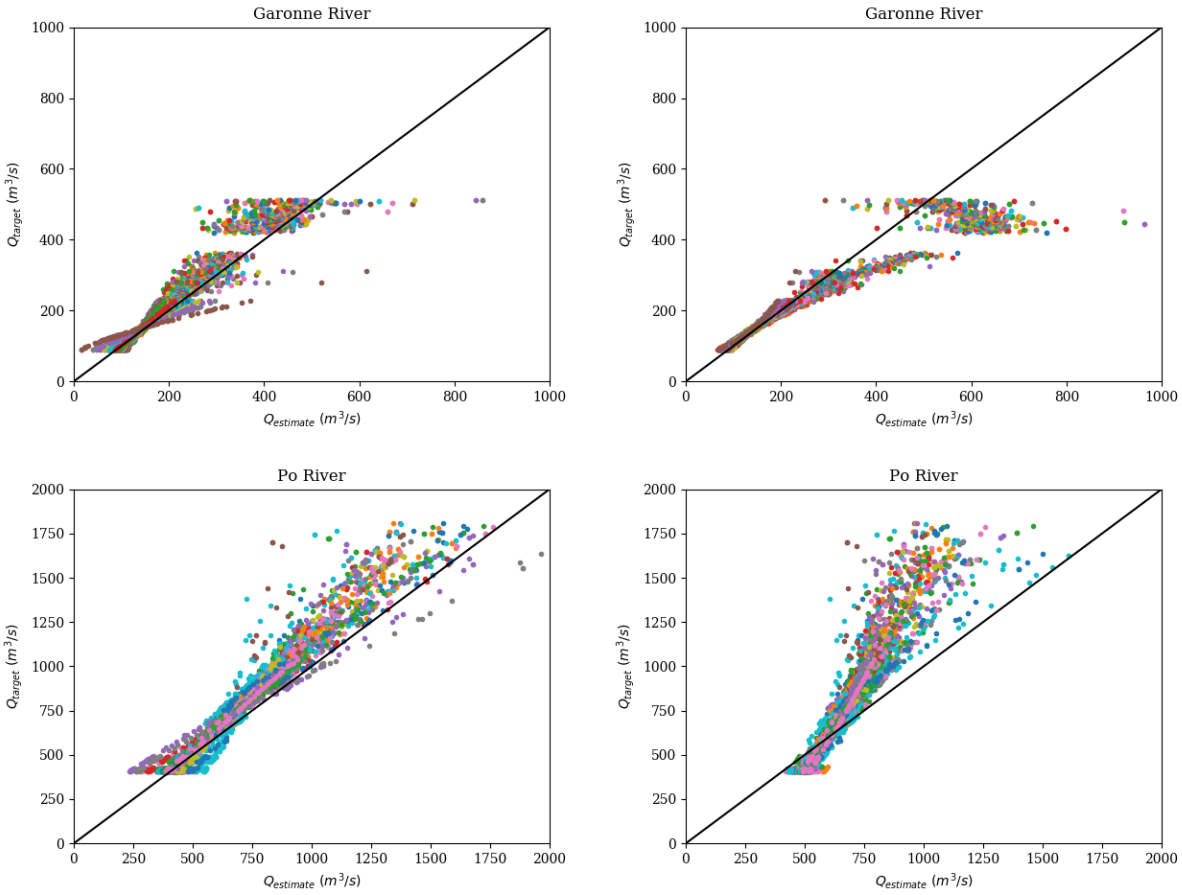

FIGURE 7.1. Discharge computations from the low complexity relations obtained after the re-calibration of the roughness K obtained by the VDA process; Plot Q_{true} vs $Q_{infered}$ using (4.1) on the complete observations set. (Top). Discharge Garonne River; (Bottom) Po River. (Left) With $K(h)$ hence K_p; (Right) With K_r.

prior information quality although the simultaneous inference of the corresponding roughness coefficient K always provides excellent effective river bottom features. Passed the hydrodynamic calibration on a complete hydrological cycle (that is a learning period of one year typically), the estimated values of $Q_{in}(t)$ and $b(x)$ obtained by the VDA process are re-employed to re-calibrate the roughness coefficient $K(x)$ corresponding to the low-complexity model (low Froude flow, locally permanent). Once this re-calibration process done, the low complexity systems make possible the estimation of the discharge *in real-time* along the newly acquired data. Finally the present inversion global algorithm can provide good estimations of worldwide river discharges which will be observed by the swath-altimetry mission SWOT. All the present equations and algorithms have been implemented into the open-source computational software DassFlow [47]. On-going investigations focus on inversions applied to larger river portions presenting lateral fluxes and complete river networks.

Authors contribution. The first author has upgraded the computational software DassFlow1D from the previous version developed by P. Brisset [11] and performed the numerical results. The second and leading author, has elaborated the low complexity equations, the computational VDA process. The third author has greatly contributed to the real data model setups and their analysis. The last author has nicely contributed to the understanding of the advanced VDA formulation (beginning of his PhD). All the authors has merged their knowledge all along the research to finally obtain the present result.

Acknowledgments. The co-authors K. Larnier (Res. Eng. CS corp.) and J. Verley (Eng. 16-17 then PhD student IMT-INSA 17-18) have been co-funded by CNES. The two other authors have been partly supported by CNES TOSCA research project 14-18. The authors acknowledge M. Durand from Ohio State University for providing the Sacramento SWOT-HR dataset. Also H. Roux from IMFT and INPT-Toulouse University has provided a fine expertise on the Garonne River dataset.

REFERENCES

[1] G. H. Allen and T. M. Pavelsky. Patterns of river width and surface area revealed by the satellite-derived north american river width data set. *Geophysical Research Letters*, 42(2):395–402, 2015.

[2] K. Andreadis, G. Schumann, and T. Pavelsky. A simple global river bankfull width and depth database. *Water Resources Research*, 49(10):7164–7168, 2013.
[3] G. Aronica, B. Hankin, and K. Beven. Uncertainty and equifinality in calibrating distributed roughness coefficients in a flood propagation model with limited data. *Advances in Water Resources*, 22(4):349 – 365, 1998.
[4] E. Bélanger and A. Vincent. Data assimilation (4d-var) to forecast flood in shallow-waters with sediment erosion. *Journal of Hydrology*, 300(14):114 – 125, 2005.
[5] S. Biancamaria, K. M. Andreadis, M. Durand, E. A. Clark, E. Rodriguez, N. M. Mognard, D. E. Alsdorf, D. P. Lettenmaier, and Y. Oudin. Preliminary characterization of SWOT hydrology error budget and global capabilities. *Selected Topics in Applied Earth Observations and Remote Sensing, IEEE Journal of*, 3:6–19, 2010. 1.
[6] S. Biancamaria, M. Durand, K.M. Andreadis, P.D. Bates, A. Boone, N.M. Mognard, E. Rodriguez, D.E. Alsdorf, D.P. Lettenmaier, and E.A. Clark. Assimilation of virtual wide swath altimetry to improve arctic river modeling. *Remote Sensing of Environment*, 115(2):373 – 381, 2011.
[7] S. Biancamaria, D. P. Lettenmaier, and T. Pavelsky. The swot mission and its capabilities for land hydrology. *Surveys in Geophysics*, 37(2):307–337, Mar 2016.
[8] D. M. Bjerklie. Estimating the bankfull velocity and discharge for rivers using remotely sensed river morphology information. *Journal of hydrology*, 341(3):144–155, 2007.
[9] D. M. Bjerklie, C. M. Birkett, J. A. Rover, J. W. Jones, J. W. Fulton, P.-A. Garambois, and J. T. Minear. Satellite remote sensing determination of river discharge: Application to the yukon river alaska. *Submitted*.
[10] F Bouttier and P Courtier. Data assimilation concepts and methods march 1999. *Meteorological training course lecture series. ECMWF*, page 59, 2002.
[11] P. Brisset, J. Monnier, P.-A. Garambois, and H. Roux. On the assimilation of altimetric data in 1d saint-venant river flow models. *Adv. Water Ress. In revision*, 2018.
[12] S. Calmant, J.-F. Cretaux, and F. Remy. 4 - principles of radar satellite altimetry for application on inland waters. In Nicolas Baghdadi and Mehrez Zribi, editors, *Microwave Remote Sensing of Land Surface*, pages 175 – 218. Elsevier, 2016.
[13] M. Carlier. *Hydraulique générale et appliquée*. Eyrolles, Paris, France, 1982.
[14] W. Castaings, D. Dartus, M. Honnorat, F.-X. Le Dimet, Y. Loukili, and J. Monnier. Automatic differentiation: a tool for variational data assimilation and adjoint sensitivity analysis for flood modeling. In *Automatic Differentiation: Applications, Theory, and Implementations*, pages 249–262. Springer, 2006.
[15] DL Chertok and RW Lardner. Variational data assimilation for a nonlinear hydraulic model. *Applied mathematical modelling*, 20(9):675–682, 1996.
[16] V.T. Chow. Handbook of applied hydrology. *McGraw-Hill Book Co., New-York, 1467 pages*, 1964.
[17] S. Cohen, A. Kettner, and J. Syvitski. Global suspended sediment and water discharge dynamics between 1960 and 2010: Continental trends and intra-basin sensitivity. *Global and Planetary Change*, 115:44 – 58, 2014.
[18] J. A. Cunge, M. Holly, F., and A. Verwey. *Practical Aspects of Computational River Hydraulics*. Pitam Publishing, 1980.
[19] Cacuci DG., Navon IM., and Ionescu-Bugor M. *Computational Methods for Data Evaluation and Assimilation*. Taylor and Francis CRC Press: Boca Raton, 2013.
[20] G. Di Baldassarre, G. Schumann, and P. Bates. Near real time satellite imagery to support and verify timely flood modelling. *Hydrological Processes*, 23(5):799–803.
[21] M. Durand, CJ. Gleason, P-A. Garambois, D. Bjerklie, LC. Smith, H. Roux, E. Rodriguez, PD. Bates, TM. Pavelsky, J Monnier, et al. An intercomparison of remote sensing river discharge estimation algorithms from measurements of river height, width, and slope. *Water Resources Research*, 2016.
[22] M. Durand, J. Neal, E. Rodríguez, K. M Andreadis, L. C. Smith, and Y. Yoon. Estimating reach-averaged discharge for the river severn from measurements of river water surface elevation and slope. *Journal of Hydrology*, 511:92–104, 2014.
[23] C. M. Emery, A. Paris, S. Biancamaria, A. Boone, S. Calmant, P.-A. Garambois, and J. S. da Silva. Large scale hydrological model river storage and discharge correction using satellite altimetry-based discharge product. *Hydrology and Earth System Sciences Discussions*, 2017:1–54, 2017.
[24] R. Frasson, R. Wei, M. Durand, J. Minear, A. Domeneghetti, G. Schumann, B. Williams, E. Rodriguez, C. Picamilh, C. Lion, T. Pavelsky, and P.-A. Garambois. Automated river reach definition strategies: Applications for the surface water and ocean topography mission. *Water Resources Research*, 53(10):8164–8186, 2017.
[25] P-A. Garambois and J. Monnier. Inference of effective river properties from remotely sensed observations of water surface. *Advances in Water Resources*, 79:103–120, 2015.
[26] I. Gejadze and P.-O. Malaterre. Discharge estimation under uncertainty using variational methods with application to the full saint-venant hydraulic network model. *International Journal for Numerical Methods in Fluids*, 83(5):405–430, 2017. fld.4273.
[27] I Yu Gejadze and J Monnier. On a 2d âzoomâfor the 1d shallow water model: Coupling and data assimilation. *Computer methods in applied mechanics and engineering*, 196(45-48):4628–4643, 2007.
[28] A. F. Gessese, M. Sellier, E. Van Houten, and G. Smart. Reconstruction of river bed topography from free surface data using a direct numerical approach in one-dimensional shallow water flow. *Inverse Problems*, 27(2):025001, 2011.
[29] J. C. Gilbert and C. Lemaréchal. Some numerical experiments with variable-storage quasi-newton algorithms. *Mathematical programming*, 45(1-3):407–435, 1989.
[30] C.J. Gleason and L. C. Smith. Toward global mapping of river discharge using satellite images and at-many-stations hydraulic geometry. *Proceedings of the National Academy of Sciences*, 111(13):4788–4791, 2014.
[31] S. Haben, A. Lawless, and N. Nichols. Conditioning and preconditioning of the variational data assimilation problem. *Computers & Fluids*, 46(1):252–256, 2011.
[32] S. Haben, A. Lawless, and N. Nichols. Conditioning of incremental variational data assimilation, with application to the met office system. *Tellus A*, 63(4):782–792, 2011.
[33] L. Hascoët and V. Pascual. The Tapenade Automatic Differentiation tool: Principles, Model, and Specification. *ACM Transactions On Mathematical Software*, 39(3), 2013.
[34] M. Honnorat, X. Lai, F-X. le Dimet, and J. Monnier. Variational data assimilation for 2D fluvial hydraulics simulation. *CMWR XVI-Computational Methods for Water Ressources. Copenhagen, june 2006.*, 2006.
[35] M. Honnorat, J. Monnier, and F.-X. Le Dimet. Lagrangian data assimilation for river hydraulics simulations. *Computing and Visualization in Science*, 12(5):235–246, 2009.
[36] M. Honnorat, J. Monnier, N. Rivière, E. Huot, and F.-X. Le Dimet. Identification of equivalent topography in an open channel flow using lagrangian data assimilation. *Computing and visualization in science*, 13(3):111–119, 2010.

[37] R. Hostache, X. Lai, J Monnier, and C. Puech. Assimilation of spatially distributed water levels into a shallow-water flood model. Part II: Use of a remote sensing image of Mosel River. *Journal of Hydrology*, 390:257–268, 2010. 3-4.
[38] B. Kaltenbacher, A. Neubauer, and O. Scherzer. *Iterative regularization methods for nonlinear ill-posed problems*, volume 6. Walter de Gruyter, 2008.
[39] X. Lai and J. Monnier. Assimilation of spatially distributed water levels into a shallow-water flood model. Part I: mathematical method and test case. *Journal of Hydrology*, 377:1–11, 2009. 1-2.
[40] K. Larnier. *Modélisation thermohydraulique d'un tronçon de Garonne en lien avec l'habitat piscicole : Approches statistique et déterministe*. PhD thesis, Toulouse, 2010.
[41] F.-X. Le Dimet and O. Talagrand. Variational algorithms for analysis and assimilation of meteorological observations: theoretical aspects. *Tellus A: Dynamic Meteorology and Oceanography*, 38(2):97–110, 1986.
[42] L. B. Leopold and T. J Maddock. The hydraulic geometry of stream channels and some physiographic implications. *USGS Numbered Series*, 252:57pp, 1953. -.
[43] J.-L. Lions. Optimal control of systems governed by partial differential equations problèmes aux limites. 1971.
[44] A. Lorenc, S. Ballard, R. Bell, N. Ingleby, P. Andrews, D. Barker, J. Bray, A. Clayton, T. Dalby, D. Li, et al. The met. office global three-dimensional variational data assimilation scheme. *Quarterly Journal of the Royal Meteorological Society*, 126(570):2991–3012, 2000.
[45] J. Marin and J. Monnier. Superposition of local zoom models and simultaneous calibration for 1d–2d shallow water flows. *Mathematics and Computers in Simulation*, 80(3):547–560, 2009.
[46] J. Monnier. *Variational data assimilation: from optimal control to large scale data assimilation*. Open Online Course, INSA Toulouse, 2014.
[47] J. Monnier, P. Brisset, K. Larnier, and P-A. Garambois. Dassflow: Data assimilation for free surface flows. Technical report, Mathematics Institute of Toulouse -INSA-CNES-CNRS-ICUBE. http://www.math.univ-toulouse.fr/DassFlow, 2018.
[48] J. Monnier, F. Couderc, D. Dartus, K. Larnier, R. Madec, and J-P. Vila. Inverse algorithms for 2D shallow water equations in presence of wet dry fronts. application to flood plain dynamics. *Advances in Water Resources*, 97:11–24, 2016.
[49] S. Munier, A. Polebistki, C. Brown, G. Belaud, and D. P. Lettenmaier. Swot data assimilation for operational reservoir management on the upper niger river basin. *Water Resources Research*, 51(1):554–575, 2015.
[50] I. Navon. Practical and theoretical aspects of adjoint parameter estimation and identifiability in meteorology and oceanography. *Dynamics of Atmospheres and Oceans*, 27(1):55 – 79, 1998.
[51] C. Ottlœ and J.-M. Mahfouf. Data assimilation of satellite observations. In N. Baghdadi and M. Zribi, editors, *Microwave Remote Sensing of Land Surface*, pages 357–382. Elsevier, 2016.
[52] H. Oubanas, I. Gejadze, P.-O. Malaterre, and F. Mercier. River discharge estimation from synthetic swot-type observations using variational data assimilation and the full saint-venant hydraulic model. *Journal of Hydrology*, pages Accepted, to appear, 2018.
[53] D. Paiva, W. Collischonn, M.-P. Bonnet, F. Frappart, S. Calmant, and C. Bulhques Mendes. Largeâscale hydrologic and hydrodynamic modeling of the amazon river basin. *Water Resources Research*, 49(3):1226–1243.
[54] R. Paiva, W. Collischonn, and C. Tucci. Large scale hydrologic and hydrodynamic modeling using limited data and a gis based approach. *Journal of Hydrology*, 406(3-4):170–181, 2011.
[55] V.G. Panchang and J.J. O'Brien. On the determination of hydraulic model parameters using the adjoint state formulation. *Modeling marine system*, 1:5–18, 1989.
[56] S. Ricci, A. Piacentini, O. Thual, E. Le Pape, and G. Jonville. Correction of upstream flow and hydraulic state with data assimilation in the context of flood forecasting. *Hydrol. Earth Syst. Sci.*, 15:3555–3575, 2011. 11.
[57] E. Rodríguez. SWOT Science requirements document. JPL document, JPL, 2012.
[58] W. Rogers. Central valley floodplain evaluation and delineation. Document, 2014.
[59] H. Roux and D. Dartus. Use of parameter optimization to estimate a flood wave: Potential applications to remote sensing of rivers. *J. of Hydrology*, 328:258–266, 2006.
[60] B.F. Sanders and N.D. Katopodes. Control of canal flow by adjoint sensitivity method. *Journal of irrigation and drainage engineering*, 125(5):287–297, 1999.
[61] Y. Sasaki. *Some basic formalisms in numerical variational analysis*. Citeseer, 1970.
[62] J. Schellekens, E. Dutra, A. Martínez-de la Torre, G. Balsamo, A. van Dijk, F. Sperna Weiland, M. Minvielle, J.-C. Calvet, B. Decharme, S. Eisner, G. Fink, M. Flörke, S. Peßenteiner, R. van Beek, J. Polcher, H. Beck, R. Orth, B. Calton, S. Burke, W. Dorigo, and G. P. Weedon. A global water resources ensemble of hydrological models: the earth2observe tier-1 dataset. *Earth System Science Data*, 9(2):389–413, 2017.
[63] A. Tarantola. *Inverse problem theory and methods for model parameter estimation*, volume 89. SIAM, 2005.
[64] J-P. Vila. *Théorie et approximation numérique de problèmes hyperboliques non linéaires applications aux équations de Saint-Venant et à la modélisation des avalanches de neige dense*. PhD thesis, Université Paris VI, March 1986.
[65] D. Wisser, B. Fekete, C Vörösmarty, and A Schumann. Reconstructing 20th century global hydrography: a contribution to the global terrestrial network-hydrology (gtn-h). *Hydrology and Earth System Sciences*, 14(1):1, 2010.
[66] Y. Yoon, M. Durand, C.J. Merry, E.A. Clark, K.M. Andreadis, and Alsdorf D.E. Estimating river bathymetry from data assimilation of synthetic swot measurements. *Journal of Hydrology*, 464 - 465(0):363 – 375, 2012.
[67] Y. Yoon, P-A. Garambois, R. Paiva, M. Durand, H. Roux, and E. Beighley. Improved error estimates of a discharge algorithm for remotely sensed river measurements: Test cases on Sacramento and Garonne Rivers. *Water Resources Research*, 52(1):278–294, 2016.